2022 American Control Conference (ACC)
Atlanta, USA, June 8-10, 2022

A weakly nonlinear analysis of transition in a hypersonic flow

Anubhav Dwivedi and Mihailo R. Jovanović

Abstract— **We study responses of compressible Navier-Stokes equations to unsteady exogenous disturbances in a hypersonic flow over a double-wedge geometry. Our analysis of the laminar shock-boundary layer interaction reveals strong amplification of upstream disturbances with non-zero temporal frequency. We utilize a weakly nonlinear framework to investigate the early stages of transition to turbulence in the presence of such unsteady disturbances. We demonstrate that quadratic interactions of harmonic perturbations induce steady three-dimensional spanwise-periodic streaks. These streaks are amplified by the flow separation and serve as a precursor to transition further downstream. Our examination of the spatial structure of the streaks demonstrates that they can be reliably reproduced via a reduced-order dynamical representation. The low-dimensional models, such as those discovered in the present study, are critically important for the development of control-oriented models for transition to turbulence in hypersonic flows.**

I. Introduction

Hypersonic flows over complex geometries are governed by compressible Navier-Stokes (NS) equations. Such flows move at speeds that are at least five times faster than the speed of sound and aerodynamic heating of the vehicle surface becomes a major concern: it is about five times larger in turbulent than in laminar flow [1] and it can lead to structural failure. Control-oriented modeling of flow transition is critical for vehicle performance and survivability. Since the dynamics at such extreme flow conditions are poorly understood, in this paper we analyze the dynamical properties of the compressible NS equations with spatially distributed and temporally varying external disturbances.

In realistic flow conditions, such as those encountered in wind tunnel experiments, the unsteady fluctuations in the free stream are a dominant source of external excitation [2]. Herein, we utilize the input-output framework to characterize the role of unsteady disturbances in initiating transition over a double-wedge geometry (which represents a canonical hypersonic flow configuration over a control surface). At hypersonic speeds, the flow over this geometry exhibits shock/boundary layer interaction (SBLI) [3] that involves separation and reattachment of flow close to the surface as well as a discontinuity associated with the shock system. Data from wind-tunnel experiments [4]–[6] reveal that the flow away from the wedge remains two-dimensional. However, the flow close to the wedge surface shows the presence of steady three-dimensional modification of the mean flow in the form of streaks [4], [7] that trigger transition to turbulence [8]. Thus, we investigate the development of steady 3D features around a 2D base flow over a double-wedge in the presence of unsteady external disturbances.

An input-output framework that evaluates the response (outputs) of the linearized NS equations to external sources (inputs) has been successfully employed to quantify the amplification and study the early stages of transition in low-speed channels [9], [10], boundary layers [11], [12], and jets [13]. Recent researched examined the input-output dynamics of the compressible linearized NS equations to show that hypersonic flows are extremely sensitive to upstream steady vortical disturbances [6], [14], [15]. The resulting flow response takes the form of 3D streaks [5], [16]. However, recent numerical experiments with SBLI suggest that even in the presence of unsteady excitation, the 2D flow develops streaks that breakdown to turbulence [17], [18]. To evaluate the development of steady streaks from small unsteady disturbances, we examine nonlinear development of the dominant response obtained identified by input-output analysis of the linearized NS equations. In particular, we utilize a weakly nonlinear framework to quantify the interaction of small perturbations responsible for early stages of transition.

Our presentation is organized as follows. In section II, we provide details about the flow geometry and computational setup. In section III, we present the linearized model and briefly summarize the input-output formulation. Next, we evaluate responses of the compressible Navier-Stokes equations linearized around laminar hypersonic base flow to time-harmonic three-dimensional disturbances. Section IV investigates nonlinear interactions of the dominant unsteady response of the linearized flow equations and demonstrates that the resulting interactions lead to the development of steady three-dimensional streaks. A weakly nonlinear framework is then employed to develop a reduced-order representation of the streaks in terms of the dominant input-output modes. Finally, we conclude our presentation in section V.

II. A hypersonic double-wedge flow

We consider a canonical hypersonic configuration involving a Mach 5 flow over a double-wedge. Figure 1 (a) shows the geometry and flow conditions that correspond to the experiments of [19]. We use the finite-volume compressible flow solver US3D [20] to solve the compressible NS equations in conservative form. The two-dimensional flow over double-wedge is computed using a computational grid with 249 cells in the wall-normal and 535 cells in the streamwise direction. Further details on the numerical approach can be found in our previous work [21].

Financial support from the Air Force Office of Scientific Research under award FA9550-18-1-0422 is gratefully acknowledged.

A. Dwivedi and M. R. Jovanović are with the Ming Hsieh Department of Electrical and Computer Engineering, University of Southern California, Los Angeles, CA 90089, USA. Emails: dwivedia@usc.edu, mihailo@usc.edu

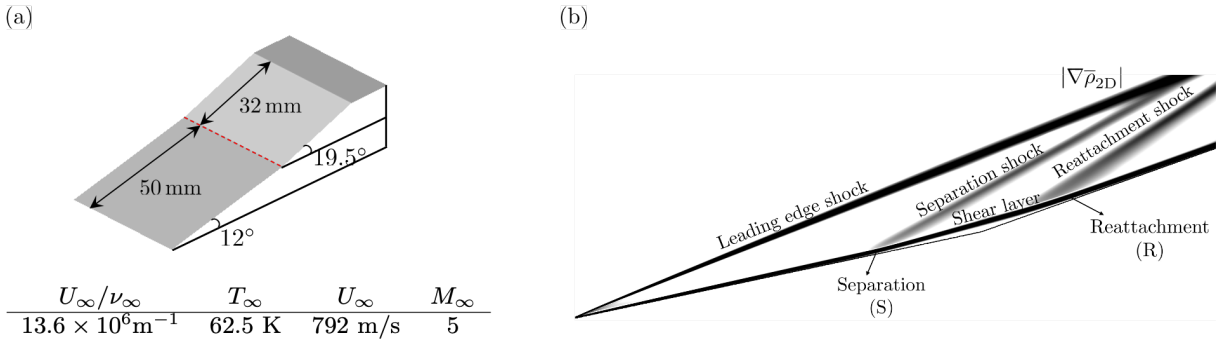

U_∞/ν_∞	T_∞	U_∞	M_∞
$13.6 \times 10^6 \mathrm{m}^{-1}$	62.5 K	792 m/s	5

Fig. 1. (a) Flow geometry and experimental conditions; (b) contours of $|\nabla\rho|$ of the two dimensional base flow.

Figure 1 (b) shows the flow features on the double-wedge with contours of density gradient magnitude $|\nabla\bar{\rho}|$. The boundary layer thickness δ near the separation location is about 1 mm. Unless otherwise specified, the length scales are non-dimensionalized by δ at the separation location, and the time-scales are non-dimensionalized by δ/U_∞, where U_∞ denotes the free-stream speed in figure 1 (a). The boundary layer separates around $13.8\,\delta$ from the corner on the first wedge and is associated with the formation of the separation shock. The separated flow reattaches around $10.5\,\delta$ away from the corner on the second wedge and the reattaching flow is associated with the formation of the reattachment shock. S and R, respectively, mark the separation and the reattachment location in the two-dimensional steady flow.

Sidharth *et al.* [21] demonstrated global linear stability of the two-dimensional separated base flow. Recent studies of similar SBLI configurations, such as compression ramps, revealed extreme sensitivity to upstream disturbances even in the absence of global instability [14]. Leading-edge roughness and free-stream disturbances provide persistent external excitation sources and are inevitable in realistic flow environments. To evaluate the role of such uncertainty in triggering the transition to turbulence, we utilize input-output (I/O) analysis [22] to quantify amplification of unsteady disturbances in hypersonic flow over the double wedge.

III. Linearized flow equations

To quantify amplification of unsteady external disturbances in globally stable two-dimensional SWBLI over a double wedge we decompose the state vector $\mathbf{U} = (\rho, \rho\mathbf{u}, E)$ into mean and fluctuating parts,

$$\mathbf{U}(\mathbf{x},t) = \mathbf{U}^{(0)}(\mathbf{x}) + \epsilon\mathbf{U}^{(1)}(\mathbf{x},t) + \cdots, \tag{1}$$

where $\mathbf{U}^{(0)}(\mathbf{x})$ represents the steady 2D laminar flow and ϵ denotes a small amplitude. To account for the rate of change of the perturbation density, momentum, and total energy, we model unsteady external disturbances as volumetric sources of excitation,

$$\mathbf{d}(\mathbf{x},t) = \epsilon\mathbf{d}^{(1)}(\mathbf{x},t). \tag{2}$$

The linearized flow equations

$$\left[\frac{\partial}{\partial t} - \mathcal{A}\left(\mathbf{U}^{(0)}\right)\right]\mathbf{U}^{(1)} = \mathcal{B}\mathbf{d}^{(1)}, \tag{3}$$

are obtained by neglecting $O(\epsilon^2)$ terms upon substitution of (1) and (2) in the compressible NS equations. Here, $\mathcal{A}(\mathbf{U}^{(0)})$ denotes the compressible NS operator resulting from linearization around the base flow $\mathbf{U}^{(0)}$ [6], [21] and $\mathcal{B}$ is the operator that specifies how disturbances enter into the state equation.

A second-order central finite-volume discretization [21] is used to obtain a finite dimensional approximation of equation (3). The state-space formulation,

$$\begin{aligned} \frac{\mathrm{d}}{\mathrm{d}t}\mathbf{q} &= \mathbf{A}\mathbf{q} + \mathbf{B}\mathbf{d}, \\ \boldsymbol{\phi} &= \mathbf{C}\mathbf{q}, \end{aligned} \tag{4}$$

describes the evolution of the spatially discretized perturbation vector $\mathbf{q}$, where $\mathbf{d}$ is a spatially distributed and temporally varying disturbance (input) and $\boldsymbol{\phi}$ is the quantity of interest (output). In equation (4), we utilize the matrix $\mathbf{B}$ to restrict the spatial location of the inputs entering into the state equation, while the matrix $\mathbf{C}$ extracts the output from the state vector $\mathbf{q}$. In the present case, $\mathbf{C}$ transforms the state $\mathbf{q}$ to output the perturbation density, velocity and temperature i.e., $\boldsymbol{\phi} = (\rho, \mathbf{u}, T)$ (see [6, appendix A.1]).

At the present flow conditions, the linearized system is globally stable and for a time-periodic input with frequency ω, $\mathbf{d}(t) = \hat{\mathbf{d}}(\omega)\mathrm{e}^{\mathrm{i}\omega t}$, the steady-state output of (4) is determined by $\boldsymbol{\phi}(t) = \hat{\boldsymbol{\phi}}(\omega)\mathrm{e}^{\mathrm{i}\omega t}$, where $\hat{\boldsymbol{\phi}}(\omega) = \mathbf{H}(\mathrm{i}\omega)\hat{\mathbf{d}}(\omega)$, $\mathbf{H}(\mathrm{i}\omega)$ is the frequency response matrix

$$\mathbf{H}(\mathrm{i}\omega) = \mathbf{C}(\mathrm{i}\omega\mathbf{I} - \mathbf{A})^{-1}\mathbf{B}, \tag{5}$$

and $\mathbf{R}(\mathrm{i}\omega) = (\mathrm{i}\omega\mathbf{I} - \mathbf{A})^{-1}$ is the resolvent associated with the linearized model (4). At any ω, the singular value decomposition of $\mathbf{H}(\mathrm{i}\omega)$ can be used to quantify amplification of time-periodic inputs [9], [22], [23],

$$\hat{\boldsymbol{\phi}}(\omega) = \mathbf{H}(\mathrm{i}\omega)\hat{\mathbf{d}}(\omega) = \sum_i \sigma_i(\omega)\boldsymbol{\phi}_i(\omega)\langle\mathbf{d}_i(\omega), \hat{\mathbf{d}}(\omega)\rangle_E. \tag{6}$$

Here, $\sigma_i(\omega)$ denotes the ith singular value of $\mathbf{H}(\mathrm{i}\omega)$, $\langle\cdot,\cdot\rangle_E$ is the inner product that induces a compressible energy norm [24] (see appendix V-A), and $\mathbf{d}_i(\omega)$ and $\boldsymbol{\phi}_i(\omega)$ are the left and right singular vectors of $\mathbf{H}(\mathrm{i}\omega)$ which provide orthonormal bases of the corresponding input and output spaces (with respect to $\langle\cdot,\cdot\rangle_E$). The frequency response $\mathbf{H}(\mathrm{i}\omega)$ maps

the ith input mode $\mathbf{d}_i(\omega)$ into the response whose spatial profile is specified by the ith output mode $\boldsymbol{\phi}_i(\omega)$ and the amplification is determined by the corresponding singular value $\sigma_i(\omega)$; i.e., for $\hat{\mathbf{d}}(\omega) = \mathbf{d}_i(\omega)$, $\hat{\boldsymbol{\phi}}(\omega) = \mathbf{H}(\mathrm{i}\omega)\mathbf{d}_i(\omega) = \sigma_i(\omega)\boldsymbol{\phi}_i(\omega)$ and $\|\hat{\boldsymbol{\phi}}(\omega)\|_E = \sigma_i(\omega)$.

For a given frequency ω, we use a matrix-free Arnoldi iterations [6], [13] to compute the singular values $\sigma_i(\omega)$ of $\mathbf{H}(\mathrm{i}\omega)$. Note that, at any ω,

$$\mathrm{G}(\omega) \;:=\; \sigma_1(\omega) \;=\; \frac{\|\mathbf{H}(\mathrm{i}\omega)\mathbf{d}_1(\omega)\|_E}{\|\mathbf{d}_1(\omega)\|_E} \;=\; \frac{\|\sigma_1(\omega)\boldsymbol{\phi}_1(\omega)\|_E}{\|\mathbf{d}_1(\omega)\|_E}, \tag{7}$$

determines the largest induced gain with respect to a compressible energy norm, where $(\mathbf{d}_1(\omega), \boldsymbol{\phi}_1(\omega))$ identify the spatial structure of the dominant input-output pair.

A. Frequency response analysis

We utilize I/O analysis to study the amplification of harmonic disturbances with frequency ω. Owing to homogeneity in the spanwise direction, the 3D perturbations take the form,

$$\mathbf{q}(x, y, z, t) = \hat{\mathbf{q}}(x, y, \beta, \omega)\mathrm{e}^{\mathrm{i}(\beta z + \omega t)}, \tag{8}$$

where $\beta = 2\pi/\lambda_z$ is the spanwise wavenumber. Thus, in addition to ω, the frequency response in equation (5) is also parameterized by the spanwise wavelength λ_z.

We first set $\mathbf{B} = \mathbf{I}$, i.e., we introduce inputs that excite flow at any spatial location and examine their impact on output density, velocity and temperature in the entire computational domain. Computations with 545 cells in the streamwise, 249 cells in the wall-normal direction yield grid independent results. The perturbations are attenuated as they leave the flow domain by utilizing a numerical sponge boundary condition near the leading edge ($x = 1$) and the outflow boundaries [6].

Figure 2 shows the dependence on the frequency ω and the wavelength λ_z of the I/O gain $G(\omega, \lambda_z)$. There are two major amplification regions with the respective peaks at $(\omega = 0, \lambda_z = 1.5)$ and $(\omega = 0.4, \lambda_z = 3)$. The first peak in G identifies the global maximum and the corresponding output is determined by reattachment streaks that result from steady vortical disturbances upstream of the recirculation zone. We observe selective amplification of disturbances with $\lambda_z \approx 1.5$ and low-pass filtering features over ω. The I/O gain G experiences rapid decay beyond the roll-off frequency $\omega \approx 0.4$ and it attains its largest value at $\omega = 0$. In contrast to [14], which focused on disturbances with $\omega = 0$, we examine unsteady disturbances that trigger oblique waves in the reattaching shear layer, as identified by the second peak in the I/O gain G. This amplification region takes place in a narrow band of temporal frequencies ω over a fairly broad range of spanwise wavelengths λ_z.

Even when we allow disturbances to enter the entire computational domain, the largest amplification is caused by inputs localized upstream (near the inflow), with the resulting response appearing downstream. The upstream disturbances are the most effective way to excite the flow because of the large convection velocity of the mean flow [23] and the dominant output emerges in the separated and the reattached regions of the base flow. In the next section, we utilize the downstream response to unsteady excitations to evaluate the growth of steady secondary perturbations using a weakly non-linear approach.

IV. Weakly non-linear analysis

In § III, we used the input-output analysis to identify oblique waves as the most energetic responses of the linearized flow equations in the presence of unsteady disturbances. Here, we present a framework to quantify perturbation development responsible for early stages of transition in the double-wedge flow as the unsteady waves amplify. In the presence of a pair of small external disturbance,

$$\mathbf{d}(x, y, z, t) \;=\; \epsilon\left(\mathbf{d}_+(x, y)\mathrm{e}^{\mathrm{i}\omega t} + \mathbf{d}_-(x, y)\mathrm{e}^{-\mathrm{i}\omega t}\right)\mathrm{e}^{\mathrm{i}\beta z}, \tag{9}$$

a weakly nonlinear analysis can be utilized to represent the flow state as

$$\begin{aligned}\mathbf{U}(\mathbf{x}, t) \;=\; & \mathbf{U}^{(0)}(x, y) \\ & + \epsilon(\mathbf{U}^{(1)}_+(x, y)\mathrm{e}^{\mathrm{i}\omega t} + \mathbf{U}^{(1)}_-(x, y)\mathrm{e}^{-\mathrm{i}\omega t})\,\mathrm{e}^{\mathrm{i}\beta z} \\ & + \epsilon^2\mathbf{U}^{(2)}(\mathbf{x}, t) + \mathcal{O}(\epsilon^3),\end{aligned} \tag{10}$$

where $\mathbf{d}^{(1)}_\pm$ and $\mathbf{U}^{(1)}_\pm$ are the principal oblique input-output pairs resulting from the linearized analysis in § III-A. At $\mathcal{O}(\epsilon^2)$, the fluctuation's dynamics are governed by

$$\left[\frac{\partial}{\partial t} \;-\; \mathcal{A}\left(\mathbf{U}^{(0)}\right)\right]\mathbf{U}^{(2)} \;=\; \mathcal{N}^{(2)}, \tag{11}$$

where $\mathcal{A}(\mathbf{U}^{(0)})$ denotes the compressible NS operator resulting from linearization around the base flow $\mathbf{U}^{(0)}$ and $\mathcal{N}^{(2)}$ is the nonlinear term that accounts for quadratic interactions between $\mathbf{U}^{(1)}_+$ and $\mathbf{U}^{(1)}_-$ (see appendix V-B for details). Furthermore, the quadratic nature of the nonlinear term allows us to express $\mathbf{U}^{(2)}(\mathbf{x}, t)$ as,

$$\begin{aligned}\mathbf{U}^{(2)}(\mathbf{x}, t) \;=\; & \left(\mathbf{U}^{(2)}_0(x, y)\right)\mathrm{e}^{2\mathrm{i}\beta z} \\ & + \left(\mathbf{U}^{(2)}_+(x, y)\mathrm{e}^{2\mathrm{i}\omega t} \;+\; \mathbf{U}^{(2)}_-(x, y)\mathrm{e}^{-2\mathrm{i}\omega t}\right)\mathrm{e}^{2\mathrm{i}\beta z}.\end{aligned} \tag{12}$$

Previous numerical experiments of flow transition induced by unsteady perturbations in canonical fluid flow setups such as low-speed channel [8] and boundary layer [25]–[27] show that there is steady three-dimensional modification of the base flow in the form of streaks. The destabilization of the boundary layer by these streamwise streaks is a precursor to flow transition. Therefore, we analyze the dynamics of the steady component of the response at $\mathcal{O}(\epsilon^2)$ which satisfies

$$\left[\mathcal{A}\left(\mathbf{U}^{(0)}\right)\mathbf{U}^{(2)}_{\text{streak}}\right](x, y) \;=\; -\mathcal{N}^{(2)}_{\text{streak}}(x, y), \tag{13}$$

Finally, the finite-volume discretization of (13) yields,

$$\mathbf{A}\mathbf{q}^{(2)}_{\text{streak}} \;=\; -\mathbf{N}^{(2)}_{\text{streak}}, \tag{14}$$

where $\mathbf{A}$ is the dynamical generator in the linearized state-space model (4). Thus, the resolvent associated with (4) evaluated at $\omega = 0$ maps the forcing $\mathbf{N}^{(2)}_{\text{streak}}$ that arises

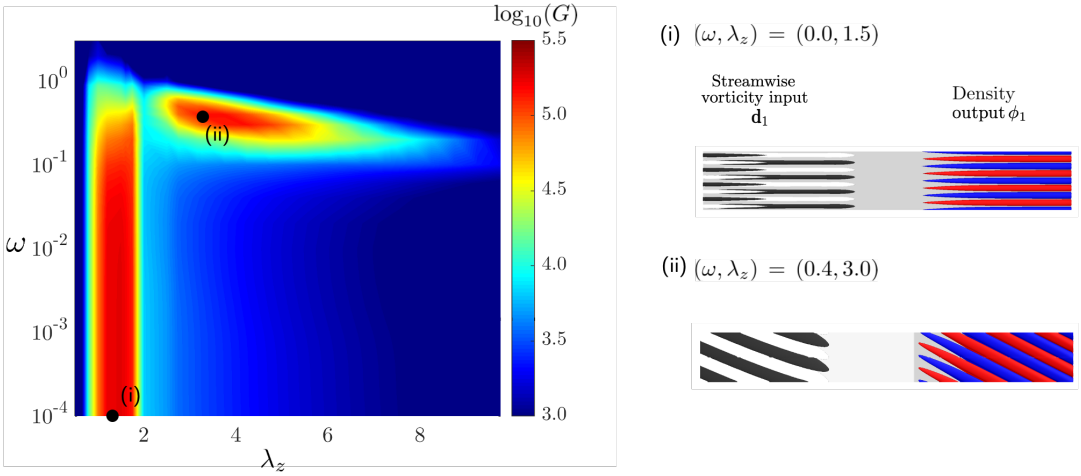

Fig. 2. Input-output analysis with $\mathbf{B} = \mathbf{C} = \mathbf{I}$. (a) Gain $G(\lambda_z, \omega)$ contours with λ_z and ω respectively. (b) Isosurfaces of streamwise vorticity corresponding to the input mode $\mathbf{d}_1$ and the temperature corresponding to the output mode ϕ_1.

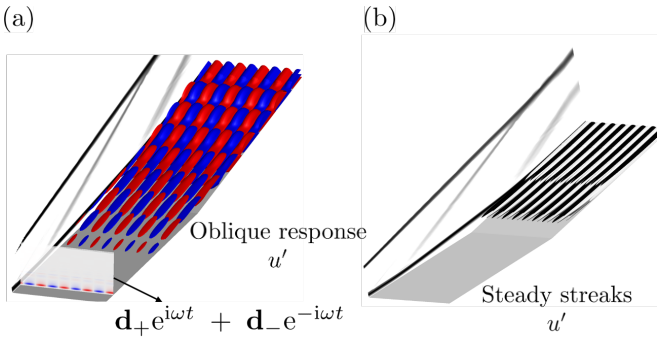

Fig. 3. (a) Setup for weakly nonlinear analysis: slice showing the dominant input mode resulting from input-output analysis at $\lambda_z = 3$ and the isosurfaces of the streamwise velocity perturbation (u') corresponding to the associated response. (b) Streamwise streaks (with $\lambda_z = 1.5$) arising from the interaction of oblique disturbances.

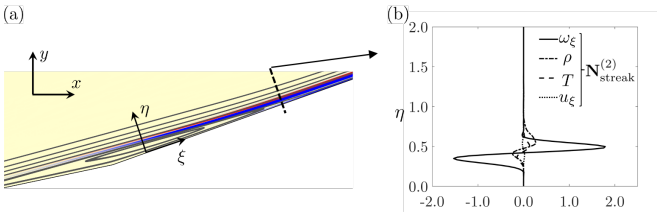

Fig. 4. (a) Real part of streamwise vorticity corresponding to $\mathbf{N}^{(2)}_{\text{streak}}$ from non-linear interaction of oblique perturbations in $x - y$ plane along with base flow streamlines. (b) Wall-normal profile of the forcing term $\mathbf{N}^{(2)}_{\text{streak}}$ to the streamwise vorticity, density, temperature, and streamwise velocity of the streaks at x = 58 (before reattachment).

from quadratic interactions of small oblique waves and yields steady streamwise streaks,

$$\mathbf{q}^{(2)}_{\text{streak}} = \mathbf{R}(\text{i}0)\mathbf{N}^{(2)}_{\text{streak}} = -\mathbf{A}^{-1}\mathbf{N}^{(2)}_{\text{streak}}. \qquad (15)$$

To investigate the emergence of streaks from upstream unsteady disturbances, we carry out the input-output analysis with streamwise localized inputs before separation, i.e. the inputs are restricted to a plane at $x = 25$ via a proper

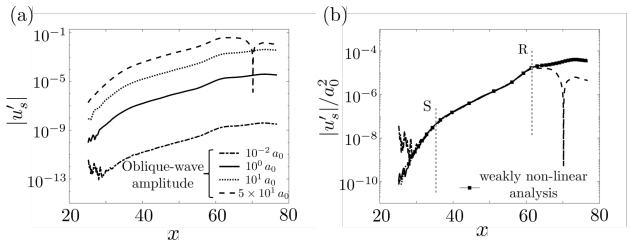

Fig. 5. (a) Streamwise velocity fluctuations associated with the steady streaks at $\lambda_z = 1.5$ from full non-linear simulations with oblique inputs with ($\omega = \pm 0.4, \lambda_z = 3$) are shown; (b) simulation results compared with the results of weakly nonlinear analysis.

selection of matrix $\mathbf{B}$. We evaluate the nonlinear evolution of the resulting dominant oblique waves. Figure 3(a) illustrates the setup in which a pair of input modes with ($\omega = \pm 0.4$, $\lambda_z = 3$) is introduced at $x_{\text{in}} = 25$. The resulting response at $\mathcal{O}(\epsilon)$ is given by oblique waves with opposite phase velocities, leading to a checkerboard wave pattern in the spanwise direction. The oblique perturbations undergo rapid amplification in the separation zone as they convect downstream. Figure 3(b) shows the steady streamwise velocity perturbations at $\mathcal{O}(\epsilon^2)$ that arise from the nonlinear interactions of the oblique waves with $\pm\omega$. The steady response is given by streamwise streaks with half the spanwise wavelength $\lambda_z^{\text{streaks}} = \lambda_z^{\text{oblique}}/2 = 1.5$ of the forcing input. These streaks experience significant amplification in the reattachment zone.

A weakly nonlinear analysis allows us to demonstrate that the source of steady streaks at $\mathcal{O}(\epsilon^2)$ arises from the quadratic interaction of oblique waves at $\mathcal{O}(\epsilon^2)$. Figure 4(a) utilizes a wall-aligned (ξ, η) coordinate system to illustrate a forcing term $\mathbf{N}^{(2)}_{\text{streak}}$ in (13). Here, ξ and η denote the directions parallel and normal to the wall, respectively. The large amplification of the oblique waves that result from the linearized analysis in the reattachment region triggers strongest forcing $\mathbf{N}^{(2)}_{\text{streak}}$ in that region. Figure 4(b) shows the wall-normal profiles of the forcing term to the mass,

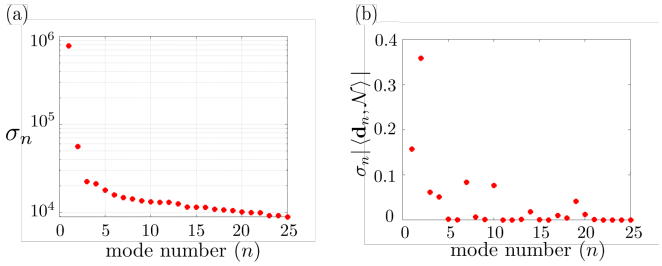

Fig. 6. (a) Dominant singular values of the linear system corresponding to the two-dimensional flow over double wedge at parameter $\lambda_z = 1.5$. (b) Projection coefficient of the input modes onto the non-linear terms from oblique wave interaction.

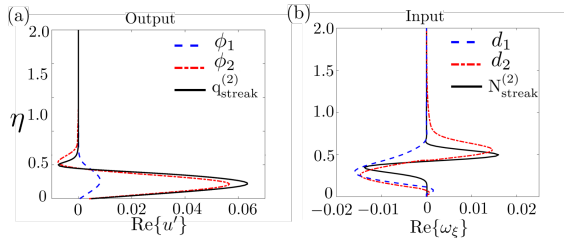

Fig. 7. Wall-normal profiles of the real component of the streamwise velocity corresponding to (a) the streaks from weakly non-linear analysis and the two dominant output modes after reattachment $x = 65$; (b) vortical forcing from the non-linear interaction of oblique waves and the two dominant input modes in the separated shear layer at $x = 57$.

momentum, and temperature equations in (11) before reattachment ($x = 58$). We observe the strongest contribution of the forcing to the wall-normal and spanwise components of the momentum equations, thereby demonstrating its vortical nature. The vortical nature is confirmed by computing the $\omega_\xi(\mathbf{N^{(2)}}) = \partial_z(v_\eta(\mathbf{N^{(2)}})) - \partial_\eta(w(\mathbf{N^{(2)}}))$. Figure 4(b) shows that $\omega_\xi(\mathbf{N^{(2)}})$ the most significant contribution to $\mathbf{N}^{(2)}_{\text{streak}}$.

To examine the validity of the second order expansion assumed in our analysis, we carry out direct numerical simulations (DNS) of NS equations forced with the oblique disturbances. Figure 5 compares the spatial evolution of the streamwise velocity perturbation of the streaks in the DNS with the weakly non-linear analysis. The results from the weakly nonlinear framework are valid across a substantial range of disturbances amplitudes, clearly demonstrating the predictive power of our approach.

A. Representation of streaks in terms of output resolvent modes

As described in § III, the left and right singular vectors of the frequency response provide an orthonormal bases of input and output spaces that can be used to study the responses of the double-wedge flow to external excitations. In particular, the streaks resulting from weakly nonlinear interactions of oblique waves (cf. equation (15)) can be represented using SVD of the resolvent associated with the linearized system (4) at $\omega = 0$,

$$\mathbf{q}^{(2)}_{\text{streak}} = \mathbf{R}(\text{i}0)\mathbf{N}^{(2)}_{\text{streak}} = \sum_i \sigma_i \boldsymbol{\phi}_i \langle \mathbf{d}_i, \mathbf{N}^{(2)}_{\text{streak}} \rangle_E. \quad (16)$$

Here, σ_i is the ith singular value and $(\mathbf{d}_i, \boldsymbol{\phi}_i)$ are the corresponding input-output modes of the resolvent $\mathbf{R}(\text{i}0) = -\mathbf{A}^{-1}$. For $\lambda_z = 1.5$, the inner product $\langle \cdot, \cdot \rangle_E$ is carried over the entire flow domain in (x, y) and the product between σ_i and the projection coefficient $\langle \mathbf{d}_i, \mathbf{N}^{(2)}_{\text{streak}} \rangle_E$ quantifies the contribution of the ith output mode $\boldsymbol{\phi}_i$ to steady streaks that are triggered by weakly nonlinear interactions of oblique waves.

Figure 6(a) shows 25 largest singular values of the resolvent for the linearized system (4) with $(\omega = 0, \lambda_z = 1.5)$. Even though the principal singular value σ_1 is an order of magnitude larger than σ_2, figure 6(b) demonstrates that the second output mode $\boldsymbol{\phi}_2$ contributes most to $\mathbf{q}^{(2)}_{\text{streak}}$. Figure 7(a) shows the wall-normal profiles of the streamwise velocity component u' associated with $\mathbf{q}^{(2)}_{\text{streak}}$ and the first two output modes $(\boldsymbol{\phi}_1, \boldsymbol{\phi}_2)$ of the resolvent. We observe striking similarity between streaks generated by weakly nonlinear interactions of oblique waves and the second output mode in the post-reattachment region, at $x = 65$. Similarly, figure 7(b) compares the wall-normal shapes of the corresponding input modes $\mathbf{d}_1$ and $\mathbf{d}_2$ with the forcing $\mathbf{N}^{(2)}_{\text{streak}}$ that arises from quadratic interactions. The input modes are visualized in the reattaching shear layer, at $x = 57$, and the streamwise vorticity component of $\mathbf{d}_2$ provides a good approximation to the vortical forcing that captures interactions of unsteady oblique fluctuations.

V. Concluding Remarks

We have employed an input-output analysis to investigate the dynamics of NS equations in the presence of small unsteady disturbances in compressible boundary layer flows. Our approach utilizes global linearized dynamics to identify the spatial structure of the dominant response. The nonlinear development of the resulting flow perturbations is investigated within a weakly non-linear framework.

To demonstrate the utility of our approach in realistic flow configurations, we examine the perturbation growth in a canonical hypersonic double-wedge geometry. The I/O analysis of the linearized NS equations predicts a significant amplification of upstream steady and unsteady external disturbances. The unsteady flow response appears in the form of oblique waves. Our weakly non-linear analysis shows that oblique waves undergo a non-linear quadratic interaction to generate steady three-dimensional vortical forcing in the separated flow. The resulting secondary response appears as streamwise streaks which undergo linear amplification. Our results demonstrate that the spatial structure of the streaks can be well approximated with the I/O modes of the two-dimensional SBLI.

The I/O approach and the weakly non-linear analysis provide a useful computational framework to quantify the spatial evolution of external perturbations in shock-boundary layer interactions. Furthermore, identifying the dominant flow structures that can exhibit significant amplification in linear and non-linear regimes can provide critical physical insights into the transition process. We expect our work to motivate additional numerical and experimental studies to

help develop reduced-order models for transition prediction and effective control strategies in complex high-speed flows.

APPENDIX

A. Compressible energy norm

In the present work, we define compressible energy using Chu's norm [24]

$$\|\cdot\|_E^2 = \int_\Omega \frac{\bar{\rho}}{2}\left|\mathbf{u}'\right|^2 + \frac{\bar{p}}{2\bar{\rho}^2}\rho'^2 + \frac{\bar{\rho}C_v}{2\bar{T}}T'^2 \,\mathrm{d}\Omega, \tag{17}$$

where $(\bar{p}, \bar{\rho}, \bar{T})$ denote the base flow pressure, density and temperature, and C_v is specific heat at constant volume in the domain Ω.

B. Non-linear terms at $\mathcal{O}(\epsilon^2)$

As shown in section IV, $\mathcal{N}^{(2)}$ accounts for quadratic interactions between $\mathbf{U}_+^{(1)}$ and $\mathbf{U}_-^{(1)}$ at $\mathcal{O}(\epsilon^2)$. For steady streaks, the dominant contributions comes from $\mathbf{N}^{(2)}_{\mathrm{streak},\mathbf{u}}$,

$$\begin{aligned}\mathbf{N}^{(2)}_{\mathrm{streak},\mathbf{u}} \;=\; & -\frac{\mathrm{i}\,\omega}{\rho^{(0)}}\left(\rho_-^{(1)}\mathbf{u}_+^{(1)} + \rho_+^{(1)}\mathbf{u}_-^{(1)}\right) - \\ & \left(\mathbf{u}_-^{(1)}\cdot\nabla\mathbf{u}_+^{(1)} + \mathbf{u}_+^{(1)}\cdot\nabla\mathbf{u}_-^{(1)}\right) - \\ & \frac{\rho_+^{(1)}}{\rho^{(0)}}\left((\mathbf{u}_-^{(1)}\cdot\nabla)\mathbf{u}^{(0)} + (\mathbf{u}^{(0)}\cdot\nabla)\mathbf{u}_-^{(1)}\right) - \\ & \frac{\rho_-^{(1)}}{\rho^{(0)}}\left((\mathbf{u}_+^{(1)}\cdot\nabla)\mathbf{u}^{(0)} + (\mathbf{u}^{(0)}\cdot\nabla)\mathbf{u}_+^{(1)}\right).\end{aligned} \tag{18}$$

Here, $\omega = 0.4$ for oblique fluctuations. For expressions for density and thermal components of $\mathbf{N}^{(2)}_{\mathrm{streak}}$ see [18, appendix D].

REFERENCES

[1] E. Reshotko, "Transition issues for atmospheric entry," *Journal of Spacecraft and Rockets*, vol. 45, no. 2, pp. 161–164, 2008.

[2] S. P. Schneider, "Developing mechanism-based methods for estimating hypersonic boundary-layer transition in flight: The role of quiet tunnels," *Prog. in Aero. Sc.*, vol. 72, pp. 17–29, 2015.

[3] G. Simeonides and W. Haase, "Experimental and computational investigations of hypersonic flow about compression ramps," *J. Fluid Mech.*, vol. 283, pp. 17–42, 1995.

[4] A. Roghelia, P. Chuvakhov, H. Olivier, and I. Egorov, "Experimental investigation of Görtler vortices in hypersonic ramp flows behind sharp and blunt leading edges," *47th AIAA Fluid Dynamics Conference*, 2017, aIAA 2017-3463.

[5] A. Dwivedi, C. J. Broslawski, G. V. Candler, and R. D. Bowersox, "Three-dimensionality in shock/boundary layer interactions: a numerical and experimental investigation," in *AIAA AVIATION 2020 FORUM*, 2020, p. 3011.

[6] A. Dwivedi, "Global input-output analysis of flow instabilities in high-speed compressible flows," Ph.D. dissertation, University of Minnesota, 2020.

[7] A. Dwivedi, J. W. Nichols, M. R. Jovanović, and G. V. Candler, "Optimal spatial growth of streaks in oblique shock/boundary layer interaction," in *8th AIAA Theoretical Fluid Mechanics Conference*, 2017, aIAA 2017-4163.

[8] P. J. Schmid and D. S. Henningson, *Stability and transition in shear flows*. New York: Springer-Verlag, 2001.

[9] M. R. Jovanović, "Modeling, analysis, and control of spatially distributed systems," Ph.D. dissertation, University of California, Santa Barbara, 2004.

[10] M. R. Jovanović and B. Bamieh, "Componentwise energy amplification in channel flows," *J. Fluid Mech.*, vol. 534, pp. 145–183, 2005.

[11] D. Sipp and O. Marquet, "Characterization of noise amplifiers with global singular modes: the case of the leading-edge flat-plate boundary layer," *Theoretical and Computational Fluid Dynamics*, vol. 27, no. 5, pp. 617–635, 2013.

[12] W. Ran, A. Zare, M. J. P. Hack, and M. R. Jovanović, "Stochastic receptivity analysis of boundary layer flow," *Phys. Rev. Fluids*, vol. 4, no. 9, p. 093901 (28 pages), September 2019.

[13] J. Jeun, J. W. Nichols, and M. R. Jovanović, "Input-output analysis of high-speed axisymmetric isothermal jet noise," *Phys. Fluids*, vol. 28, no. 4, p. 047101, 2016.

[14] A. Dwivedi, G. S. Sidharth, J. W. Nichols, G. V. Candler, and M. R. Jovanović, "Reattachment vortices in hypersonic compression ramp flow: an input-output analysis," *J. Fluid Mech.*, vol. 880, pp. 113–135, December 2019.

[15] A. Dwivedi, G. V. Candler, and M. R. Jovanović, "A frequency domain analysis of compressible linearized navier-stokes equations in a hypersonic compression ramp flow," in *2020 American Control Conference (ACC)*. IEEE, 2020, pp. 4325–4330.

[16] G. Sidharth, A. Dwivedi, J. Nichols, M. Jovanović, and G. Candler, "Global linear stability and sensitivity of hypersonic shock-boundary layer interactions," in *IUTAM Laminar-Turbulent Transition*. Springer, 2022, pp. 489–498.

[17] M. Lugrin, S. Beneddine, C. Leclercq, E. Garnier, and R. Bur, "Transition scenario in hypersonic axisymmetrical compression ramp flow," *J Fluid Mech.*, vol. 907, p. A6, 2021.

[18] A. Dwivedi, G. S. Sidharth, and M. R. Jovanović, "Oblique transition in hypersonic double-wedge flow: An input-output viewpoint," *J. Fluid Mech.*, 2021, submitted; also arXiv:2111.15153.

[19] L. Yang, H. Zare-Behtash, E. Erdem, and K. Kontis, "Investigation of the double ramp in hypersonic flow using luminescent measurement systems," *Exp. Therm. Fluid Sci.*, vol. 40, pp. 50–56, 2012.

[20] G. V. Candler, H. B. Johnson, I. Nompelis, V. M. Gidzak, P. K. Subbareddy, and M. Barnhardt, "Development of the US3D code for advanced compressible and reacting flow simulations," in *53rd AIAA Aerospace Sciences Meeting*, 2015, aIAA 2015-1893.

[21] G. S. Sidharth, A. Dwivedi, G. V. Candler, and J. W. Nichols, "Onset of three-dimensionality in supersonic flow over a slender double wedge," *Phys. Rev. Fluids*, vol. 3, no. 9, p. 093901, 2018.

[22] M. R. Jovanović, "From bypass transition to flow control and data-driven turbulence modeling: An input-output viewpoint," *Annu. Rev. Fluid Mech.*, vol. 53, no. 1, pp. 311–345, January 2021.

[23] P. J. Schmid, "Nonmodal stability theory," *Annu. Rev. Fluid Mech.*, vol. 39, pp. 129–162, 2007.

[24] A. Hanifi, P. J. Schmid, and D. S. Henningson, "Transient growth in compressible boundary layer flow," *Phys. Fluids*, vol. 8, no. 3, pp. 826–837, 1996.

[25] C.-L. Chang and M. R. Malik, "Oblique-mode breakdown and secondary instability in supersonic boundary layers," *J. Fluid Mech.*, vol. 273, p. 323–360, 1994.

[26] S. Berlin and D. S. Henningson, "A nonlinear mechanism for receptivity of free-stream disturbances," *Phys. Fluids*, vol. 11, no. 12, pp. 3749–3760, 1999.

[27] C. S. J. Mayer, D. A. Von Terzi, and H. F. Fasel, "Direct numerical simulation of complete transition to turbulence via oblique breakdown at mach 3," *J. Fluid Mech.*, vol. 674, p. 5, 2011.